

Non- d^0 Mn-driven ferroelectricity in antiferromagnetic BaMnO₃

James M. Rondinelli,* Aaron S. Eidelson, and Nicola A. Spaldin
Materials Department, University of California, Santa Barbara, CA, 93106-5050, USA
(Dated: August 20, 2018)

Using first-principles density functional theory we predict a ferroelectric ground state – driven by off-centering of the magnetic Mn⁴⁺ ion – in perovskite-structure BaMnO₃. Our finding is surprising, since the competition between energy-lowering covalent bond formation, and energy-raising Coulombic repulsions usually only favors off-centering on the perovskite *B*-site for non-magnetic d^0 ions. We explain this tendency for ferroelectric off-centering by analyzing the changes in electronic structure between the centrosymmetric and polar states, and by calculating the Born effective charges; we find anomalously large values for Mn and O consistent with our calculated polarization of 12.8 $\mu\text{C}/\text{cm}^2$. Finally, we suggest possible routes by which the perovskite phase may be stabilized over the usual hexagonal phase, to enable a practical realization of a single-phase multiferroic.

PACS numbers: 71.15.Mb, 71.20.-b, 75.47.Lx, 77.80.-e

Almost sixty years ago, Matthias observed that ferroelectricity occurs in the *ABO*₃ perovskite structure when the *B*-site is a transition metal cation with a non-magnetic d^0 electronic structure.¹ Since then, many such d^0 perovskite ferroelectric compounds have been identified, and the requirement for “ d^0 -ness” has been explained in terms of covalent bond formation between empty transition metal *d* and filled O *2p* orbitals.^{2,3} This *Matthias rule* is problematic however for the design of new multiferroic perovskites, since magnetism is most readily accommodated in the perovskite structure by partial occupation of the transition metal *d* orbitals. Indeed, the contra-indication between *B*-site ferroelectricity and *B*-site magnetism⁴ has prompted the search for and identification of new mechanisms for ferroelectricity, which do not involve *B*-site cation off-centering: these include lone pair stereochemical activity,⁵ spin spirals,⁶ charge ordering,⁷ and geometric ferroelectricity.⁸ In this work we discuss instead the circumstances under which the Matthias rule can be circumvented and magnetic *B*-site ions can be made to off-center, using perovskite-structure barium manganite as our example.

We begin this report with a review of the physics of the second order Jahn-Teller effect, which explains why a non-centrosymmetric distortion – required for ferroelectricity – is usually only favorable for d^0 transition metal cations. Then we discuss the balance between ferroelectric and competing non-ferroelectric distortions, which in perovskite oxides are often rotations of the oxygen octahedra. The main part of the paper is a detailed first-principles study of BaMnO₃ in the metastable perovskite structure: We find a ferroelectric ground state, with a substantial ferroelectric polarization, driven by off-centering of the magnetic Mn⁴⁺ ion. Finally, we discuss possibilities for realizing this structure experimentally.

The tendency of a material to ferroelectric instability can be understood within the framework of vibronic coupling theory,⁹ where it appears as the second-order terms in the perturbative expansion of the total energy with respect to distortions from a high symmetry ref-

erence phase. As a result it is often called the second-order Jahn-Teller (SOJT) effect. Expanding the Hamiltonian as a function of normal coordinate *Q* about the electronic Hamiltonian for the high symmetry reference phase, $\mathcal{H}^{(0)}$, gives

$$\mathcal{H} = \mathcal{H}^{(0)} + \mathcal{H}^{(1)}Q + \frac{1}{2}\mathcal{H}^{(2)}Q^2 + \dots \quad , \quad (1)$$

with

$$\mathcal{H}^{(1)} = \left. \frac{\delta\mathcal{H}}{\delta Q} \right|_{Q=0} \quad \text{and} \quad \mathcal{H}^{(2)} = \left. \frac{\delta^2\mathcal{H}}{\delta Q^2} \right|_{Q=0} \quad .$$

$\mathcal{H}^{(1)}$ and $\mathcal{H}^{(2)}$ capture the vibronic coupling between the displacements of the ions from their positions in the high symmetry phase and the electrons. Using standard perturbation theory, the energy can be expanded as a function of the normal coordinate about the high symmetry reference structure^{10,11} with energy $E^{(0)}$ as

$$\begin{aligned} E &= E^{(0)} + \langle 0 | \mathcal{H}^{(1)} | 0 \rangle Q \\ &+ \frac{1}{2} [\langle 0 | \mathcal{H}^{(2)} | 0 \rangle - 2 \sum_n \frac{|\langle 0 | \mathcal{H}^{(1)} | n \rangle|^2}{E^{(n)} - E^{(0)}}] Q^2 \\ &+ \dots \end{aligned} \quad (2)$$

Here $|0\rangle$ is the the lowest energy solution of $\mathcal{H}^{(0)}$ and the $|n\rangle$ s are excited states with energies $E^{(n)}$. The first-order term, $\langle 0 | \mathcal{H}^{(1)} | 0 \rangle Q$, describes the regular first-order Jahn-Teller theorem. This term is non-zero only for orbitally degenerate states, and in the case of *d* orbitals it always leads to centrosymmetric distortions, therefore it does not give rise to ferroelectricity. Note, however, that in cases where it is non-zero it dominates over any non-centrosymmetric second-order distortions.

In non-orbitally degenerate systems, competition between the two second-order terms, which are of opposite sign, determines whether a non-centrosymmetric off-centering is favored or not. The first of the two second-order terms describes the short-range repulsive forces which would result if the ions were displaced with

the electrons frozen in their high symmetry configuration. Since $\langle 0 | \mathcal{H}^{(2)} | 0 \rangle$ is always positive, it always raises the energy of the system, and so polar distortions are more likely to be favored if this term is small; this tends to be the case for closed-shell d^0 cations without valence electrons. The second of the second-order terms, $-\sum_n \frac{|\langle 0 | \mathcal{H}^{(1)} | n \rangle|^2}{E^{(n)} - E^{(0)}} Q^2$, describes the relaxation of the electronic system in response to the ionic displacements through covalent bond formation. It is always negative unless it is zero by symmetry, and so it favors ferroelectricity when its magnitude is large for non-centrosymmetric distortions. This occurs when the products of the ground and lowest excited states are of odd parity, so that the matrix elements are non-zero in the cases when $E^{(n)} - E^{(0)}$ is small. For Mott insulators with partially filled d shells, the top of the valence band and bottom of the conduction band are both composed primarily of transition metal d states. Therefore the ground and low-lying excited states have the same symmetry, their product with $\mathcal{H}^{(1)}$ is odd, and the matrix element $\langle 0 | \mathcal{H}^{(1)} | n \rangle$ is zero. Conversely, for d^0 perovskites, the top of the valence band is made up largely of O $2p$ states, and the bottom of the conduction band of transition metal $3d$ states, thus the product of the ground and low-lying excited states with $\mathcal{H}^{(1)}$ is even, and the matrix element $\langle 0 | \mathcal{H}^{(1)} | n \rangle$ is non-zero.

Consequently, the balance between the positive and negative second-order terms usually results in off-centering for d^0 cations, such as Ti^{4+} in the prototypical ferroelectric BaTiO_3 . Here a strong increase in O $2p$ - Ti $3d$ hybridization accompanies the distortion from the high symmetry to the polar structure¹² and so the relevant $\langle 0 | \mathcal{H}^{(1)} | n \rangle$ matrix elements are large. This rearrangement of the electrons through covalent bond formation leads to Born effective charges, $Z^* = \delta P / \delta u$, which are significantly larger in magnitude than the formal charges on the ions; these are referred to as anomalous Born effective charges (BECs). An anomalous BEC is therefore a good indicator of the tendency of an ion to off-center and is often taken as a signature of ferroelectricity. The calculated BEC of Ti in the high-symmetry cubic phase of BaTiO_3 , for example, is almost +7 whereas the formal charge is +4.^{12,13} This is because, as the Ti ion moves towards an oxygen carrying its positive charge, negative electronic charge flows towards it from the oxygen ion, leading to a larger polarization than would arise from the ionic component alone. Conversely the balance between the second-order terms usually disfavors off-centering in transition metals with partially filled d shells, since in this case the repulsive Coulomb interactions are stronger than any energy gain from chemical bond formation. We note, however, that second-order Jahn-Teller behavior is referred to as an *effect*, not a theorem, because there is no fundamental requirement that the guidelines described above always hold. (In contrast, first-order Jahn-Teller is a *theorem* since it is not a competition between two terms of opposite sign.)

In addition to this competition between bond forma-

tion and Coulomb repulsion that determines the tendency for off-centering distortions, other centrosymmetric instabilities compete with ferroelectric distortions in determining the ground state. We mentioned already first-order Jahn-Teller distortions which always dominate if they are allowed by symmetry. In addition, in perovskite-structure oxides centrosymmetric antiferrodistortive rotations of the oxygen octahedra are common. When these rotational instabilities are strong – usually in cases when the A -site ionic radius is smaller than ideal for the perovskite structure – the tendency to form a polar ground state is drastically reduced even in materials with strongly anomalous B -site BECs. In fact, frustration of these rotational instabilities has been proposed as a viable route to novel ferroelectricity and multiferroic behavior.^{14,15}

In this manuscript, we use first-principles calculations to identify a material – perovskite structure BaMnO_3 – in which a polar mode with transition-metal off-centering is the dominant instability in spite of the partially filled d^3 manifold on the B -site. Our motivation for choosing perovskite BaMnO_3 is two-fold: First, CaMnO_3 , which is paraelectric down to low temperature, has long been known to have an anomalous Mn BEC,¹⁶ suggestive of a ferroelectric instability. And second, recent calculations^{17,18} for CaMnO_3 showed that ferroelectricity can be artificially stabilized by increasing the lattice constants (equivalent to applying negative hydrostatic pressure) or with tensile strain, so that the short-range repulsions are substantially reduced. Since the Ba^{2+} ion has a larger radius than Ca^{2+} , perovskite-structure BaMnO_3 is analogous to CaMnO_3 under negative pressure. We note, however, that because of the large size of Ba^{2+} , the experimental structure of BaMnO_3 is not perovskite, but rather a hexagonal phase with face-shared oxygen octahedra.¹⁹ We discuss options for stabilizing the perovskite phase at the end of the manuscript.

Our first-principles density functional calculations are performed within the local spin-density approximation (LSDA) as implemented in the Vienna *ab initio* simulation package (VASP).^{20,21} The projector augmented wave method²² is used with the following valence electron configurations: $5s^2 5p^6 6s^2$ for Ba, $3d^6 4s^1$ for Mn and $2s^2 2p^4$ for oxygen. The Brillouin zone integrations are performed with the tetrahedron method²³ over a $9 \times 9 \times 9$ Monkhorst-Pack k -point mesh²⁴ centered at Γ and a 450 eV plane-wave cutoff. For structural relaxations a Gaussian broadening technique of 0.05 eV is used and the ions are relaxed until the Hellmann-Feynman forces are less than 1 meV \AA^{-1} . The electronic contribution to the polarization is calculated following the standard Berry phase formalism.^{25,26}

We begin by determining the equilibrium volume for the hypothetical cubic (space group $Pm\bar{3}m$) BaMnO_3 structure with G -type antiferromagnetic order of the Mn^{4+} cations. This G -type antiferromagnetism is the likely ground state since both CaMnO_3 and SrMnO_3 have been shown to exhibit the same type of order

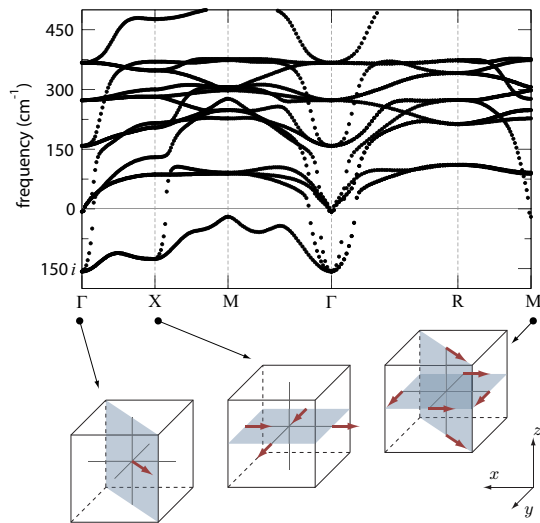


FIG. 1: Phonon dispersions of the *G*-type AFM cubic BaMnO₃ along the high-symmetry lines. Energy lowering eigenvector modes for the unstable phonons at Γ , X and M, with the Mn ion at the center of the unit cell surrounded by an oxygen octahedron.

in the perovskite phase.^{27,28} We find that the primitive equilibrium unit cell volume $\Omega_0 = 58.7 \text{ \AA}^3$ (cubic lattice parameter of $a_0 = 3.89 \text{ \AA}$) is larger than previous first-principles calculations for CaMnO₃ using various exchange-correlation functionals, consistent with the larger *A*-site cation size.^{17,29,30} The centrosymmetric structure is insulating with a LSDA band gap of 0.20 eV. (With a moderate effective Hubbard U of 4.5 eV, we find a gap of 0.26 eV). The valence band is predominantly majority spin Mn t_{2g} and O $2p$ character with strong p - d hybridization [Figure 2 (upper panels)]. The conduction band is formed by the empty Mn e_g orbitals and the minority spin t_{2g} states, which is consistent with Mn⁴⁺ in an octahedral crystal field. A local magnetic moment of $2.3 \mu_B$ is found at each Mn site, which is slightly reduced from the formal $3 \mu_B$ due to strong hybridization with the oxygen $2p$ orbitals.

We next calculate the lattice instabilities for the optimized cubic structure using the frozen-phonon method.³¹ In this method the phonons are found by calculating total energies with respect to atomic displacements from the reference structure at high symmetry positions, q , in the Brillouin zone. We use a $3 \times 3 \times 3$ (270 atom) supercell, which allows us to directly access 8 high symmetry points in the Brillouin zone by freezing in different atomic displacement patterns. For each q value we construct the dynamical matrix from the Hellman-Feynman forces induced on the ions after making small positive and negative displacements (to remove any quadratic effects) about the high symmetry positions. Diagonalization of the dynamical matrix yields the atomic displacement patterns (eigenvectors) and phonon mode frequencies (eigenvalues) at that q point. The complete phonon dispersions are then determined by interpolating these solutions of

the dynamical matrix at the special q -points to the whole Brillouin zone using a Fourier interpolation scheme.^{32,33} The splitting between the longitudinal optic (LO) and transverse optic (TO) modes at $k = 0$ is not included in our calculations.

In Figure 1, we show the phonon dispersion curves for *G*-type BaMnO₃ along the high-symmetry directions in the Brillouin zone of the primitive (5-atom) unit cell. The dominant instability is a triply degenerate Γ -point mode with an imaginary frequency of $157.2i \text{ cm}^{-1}$ and point symmetry T_{1u} . This is a polar mode consisting of a relative Mn-O displacement in which the oxygen octahedra remain almost rigid. In the ground state structure (described below) we find that this mode dominates with the Mn displacement occurring along the $[110]$ direction of the primitive cubic unit cell. Interestingly, the other high symmetry instabilities – at the X and M points – do not correspond to the usual antiferrodistortive rotations of the oxygen octahedra which are common in perovskites. The X-point mode has an imaginary frequency of $125.5i \text{ cm}^{-1}$ and A_{2u} symmetry. It corresponds to a breathing of the oxygen octahedra in the xy -plane in which two adjacent oxygens move in towards the Mn ion and two move out, so that two short and two long Mn–O bonds are created (Figure 1). In the ground state structure it combines with the T_{1u} mode with almost equal amplitude. The less unstable M-point [$\omega = 19.64i$, (E_u symmetry)] also corresponds to a distortion rather than a rotation of the oxygen octahedra, this time dominated by displacements of the apical oxygen atoms (Figure 1). We also verified that these modes are robust to correlation effects by repeating the calculations with an effective Hubbard U parameter of 4.5 eV.

Next we determined the ground state structure by freezing linear combinations of each of the unstable modes described above into the cubic $Pm\bar{3}m$ phase, then fully relaxing all internal degrees of freedom until the forces were less than 1 meV \AA^{-1} . We began with a constant volume constraint, and obtained a polar structure with $R\bar{3}m$ space group.³⁴ We then lifted the volume constraint and performed a full optimization of the atomic positions and lattice parameters within orthorhombic symmetry (20-atom unit cell). We obtained a polar ground state structure with $Amm2$ space group, and structural parameters given in Table I. The

Atom	Site	x	y	z
Ba	$2a$	0	0	0.486
Mn	$2b$	$\frac{1}{2}$	0	-0.018
O(1)	$2a$	0	0	-0.011
O(2)	$4e$	$\frac{1}{2}$	0.249	-0.260

TABLE I: Calculated structural parameters for BaMnO₃ with $Amm2$ symmetry. Our calculated lattice parameters are $a = 3.84$, $b = 5.43$, and $c = 5.43 \text{ \AA}$ with a volume per formula unit of 56.7 \AA^3 .

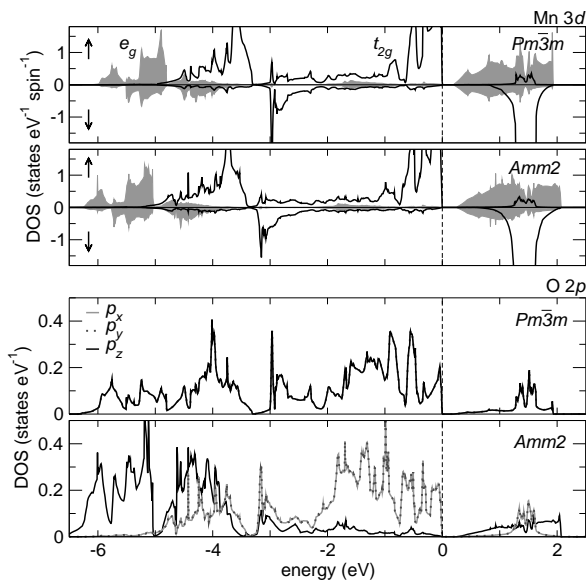


FIG. 2: Orbital resolved Mn $3d$ and O $2p$ densities of states in the centrosymmetric cubic ($Pm\bar{3}m$) and the polar ($Amm2$) structures. (Upper panels) spin-polarized DOS of a single Mn atom in the G -type AFM $BaMnO_3$ structure. (Lower panels) DOS of the O atom on top of the Mn atom. In the $Pm\bar{3}m$ structure only the p_z orbital is shown as the oxygen $2p$ orbitals are degenerate.

ground state structure is 64 meV lower in energy per formula unit than the cubic $Pm\bar{3}m$ structure. We find that our calculated ground state structure can be written as a linear combination of the unstable modes of the cubic reference structure with the following coefficients: $0.694T_{1u} + 0.604A_{2u} + 0.393E_u$. The resulting structure has three unique Mn–O bond lengths of 1.88, 1.92 and 1.96 Å with a mean Mn–O–Mn bond angle is decreased to 178.2° from the ideal 180° cubic structure.

Next, we examine the changes in the electronic structure following displacement in order to explain the stabilization of the ferroelectric off-centering of the magnetic Mn cation. In Figure 2 we compare the densities of states (DOS) for the non-polar cubic and polar $Amm2$ structures; in particular, we focus on the orbital resolved DOS for the Mn $3d$ and O $2p$ bands. The electronic structure of the metastable cubic phase was described earlier; here we reiterate that both the t_{2g} and e_g states are hybridized with the O $2p$ orbitals indicating that some covalent bonding is already present in the cubic phase. In the polar $Amm2$ ground state an increase in hybridization between the Mn e_g and O $2p$ levels occurs. This lowers the energy of the e_g states by ~ 0.30 eV, and shifts the O p_z states from the top to the bottom of the valence band; both factors result in an increase of the valence bandwidth. In terms of our earlier discussion of the SOJT effect, the matrix elements $\langle 0 | \mathcal{H}^{(1)} | n \rangle$ are large because of the enhanced Mn e_g and O $2p$ hybridization, and the ferroelectric distortion is favored.

We next calculate the total polarization for the $Amm2$ structure as the sum of the ionic and electronic contributions (including both spin channels) using the Berry’s phase method. Here we find a value of $12.8 \mu\text{C cm}^{-2}$, which is substantial compared to many manganite multiferroics,^{35,36,37} but consistent in magnitude with conventional d^0 ferroelectric perovskite oxides. We next calculate the BECs for the cubic phase along the $[111]$ direction, since large anomalies from the formal charge values are often good indicators for the underlying ferroelectric instability. In Table II we tabulate the spin-resolved BECs for each atom i decomposed such that $Z_i^* = Z_i^{\text{ion}} + Z_i^{\text{el},\uparrow} + Z_i^{\text{el},\downarrow}$, where Z_i^{ion} is the pseudocore charge. We find an anomalously large BEC for Mn, consistent with our finding of a ferroelectric instability dominated by Mn displacement. In fact we see that the majority spin electronic contribution is *positive*, corresponding to a net flow of electrons *towards* the Mn as it displaces towards the oxygen; this is consistent with the enhanced Mn–O hybridization that we observed in our calculated DOSs. [An anomalously large value is also found for Mn (8.45), when correlation effects are added, albeit reduced due to the enhanced band gap and narrowing of the e_g bandwidth.] Interestingly, the minority spin electronic contribution on the Mn ion is close to the formal charge value; this reflects the low availability of Mn minority states to accept electrons at the bottom of the conduction band in the cubic structure. In the polar $Amm2$ structure, the calculated Mn Z^* in the $[111]$ Cartesian direction is 8.34 (7.45 within the LSDA+ U method); this reduction from the cubic case is consistent with behavior in conventional perovskites and also reflects in this case the opening of the band gap between the cubic and ground state structures.

We conclude by exploring the feasibility of accessing perovskite-structure $BaMnO_3$ experimentally. As we discussed above, non-ferroelectric $CaMnO_3$ exists in the perovskite structure and is nearly cubic³⁸ with small rotations of ideal MnO_6 octahedra. Increasing the size of the A -site cation, which we have shown promotes the tendency to ferroelectric instability, also destabilizes the perovskite structure. $SrMnO_3$ is found experimen-

		Z^*	Z^{ion}	$Z^{\text{el},\uparrow}$	$Z^{\text{el},\downarrow}$
Ba	Formal	+2	10	-4	-4
	LSDA	2.72	10	-3.64	-3.64
Mn	Formal	+4	7	-3	0
	LSDA	10.22	7	+3.75	-0.53
O	Formal	-2	6	-4	-4
	LSDA	-3.97	6	-4.99	-4.98

TABLE II: Spin-resolved Born effective charges for cubic $BaMnO_3$ calculated within the LSDA along the $[111]$ direction. The spin components for Ba and O are equivalent within the numerical accuracy.

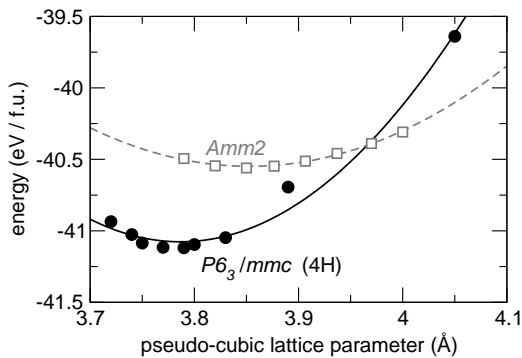


FIG. 3: Total energies for the the polar $Amm2$ and experimental 4H $BaMnO_3$ structures as a function of the pseudo-cubic lattice parameter. The lines are quadratic fits to the calculated energies.

tally in both cubic perovskite and the non-perovskite 2H hexagonal polymorphs,³⁹ while $BaMnO_3$ is known only in the denser hexagonal 4H structure with face-shared octahedra.⁴⁰ Therefore, we next calculate the relative stability of our predicted $Amm2$ perovskite-structure $BaMnO_3$ and the experimental 4H structure. Our results are shown in Figure 3, as a function of pseudo-cubic lattice parameter. We find that the experimental 4H- $BaMnO_3$ structure is more stable than the $Amm2$ perovskite structure by ~ 0.50 eV per formula unit. Only near 4.7% expansion of the 4H lattice parameter is the perovskite structure energetically favored over the 4H structure. These large energy differences suggest that experimental synthesis of the perovskite phase will be challenging, although might be feasible through epitaxial stabilization in ultra-thin films; this approach has indeed been successful in stabilizing orthorhombic, over hexagonal, rare-earth manganites.^{41,42} Another possibility is to search for a critical alloying range with Ca and/or Sr at which the perovskite structure remains stable over the 2H or 4H structure, but within the perovskite structure

where the ferroelectric instability has already started to dominate.

Finally, we note that, if a ferroelectric Ba-based perovskite manganite could be achieved experimentally, subsequent rare-earth doping on the A -site could lead to an intriguing analogy to the colossal magnetoresistive (CMR) materials. In conventional CMR materials, a phase transition between a paramagnetic insulator and a ferromagnetic metal is induced by applied magnetic field and/or temperature. In rare-earth doped $BaMnO_3$, the insulating phase might be expected to be polar, leading to a ferroelectric insulator – ferromagnetic metal transition. We suggest Ba-rich $La_{1-x}Ba_xMnO_3$ as a material for further experimental investigation.

To summarize, we have used hypothetical perovskite-structure $BaMnO_3$ to demonstrate that, in contrast to conventional wisdom, non- d^0 magnetic cations can undergo SOJT off-centering distortions resulting in polar ground states. We have explained the behavior in terms of the delicate balance between competing energies in the second-order Jahn-Teller effect, and shown that reducing Coulombic repulsions via increasing ionic separations is a general route to promoting ferroelectricity in magnetic compounds. Finally, we have explored the feasibility of realizing such novel single-phase multiferroics experimentally.

The authors thank A.J. Hatt and S. Bhattacharjee for useful discussions. This work was supported NSF under grant no. DMR-0605852 (NAS). JMR acknowledges support from NDSEG (DoD), the IMI Program of the National Science Foundation under award no. DMR04-09848, and hospitality from the Department of Advanced Materials, University of Tokyo, Kashiwanoha. ASE was supported by the Apprentice Researchers program of the CNSI at UCSB with funding from the NNIN (award no. 44771-7475). Portions of this work made use of the SGI Altix COBALT system at the National Center for Supercomputing Applications under grant no. TG-DMR-050002S.

* Address correspondence to: rondo@mrl.ucsb.edu

¹ B. T. Matthias, Phys. Rev. **75**, 1771 (1949).

² R. E. Cohen, Nature **358**, 136 (1992).

³ R. E. Cohen and H. Krakauer, Ferroelectrics **136**, 65 (1992).

⁴ N. A. Hill, J. Phys. Chem. B **104**, 6694 (2000).

⁵ R. Seshadri and N. A. Hill, Chem. Mater. **13**, 2892 (2001).

⁶ R. E. Newnham, J. J. Kramer, W. A. Schulze, and L. E. Cross, J. Appl. Phys. **49**, 6088 (1978).

⁷ N. Ikeda, H. Ohsumi, K. Ohwada, K. Ishii, T. Inami, K. Kakurai, Y. Murakami, K. Yoshii, S. Mori, Y. Horibe, et al., Nature **436**, 1136 (2005).

⁸ B. B. van Aken, T. T. M. Palstra, A. Filippetti, and N. A. Spaldin, Nature Mater. **3**, 164 (2004).

⁹ I. Bersuker, Chemical Reviews **101**, 1067 (2001).

¹⁰ J. K. Burdett, Inorg. Chem. **20**, 1959 (1981).

¹¹ R. G. Pearson, J. Molec. Struct. (THEOCHEM) **103**, 25

(1983).

¹² A. Filippetti and N. A. Hill, Phys. Rev. B **65**, 195120 (2002).

¹³ P. Ghosez, J.-P. Michenaud, and X. Gonze, Phys. Rev. B **58**, 6224 (1998).

¹⁴ D. I. Bilc and D. J. Singh, Phys. Rev. Lett. **96**, 147602 (2006).

¹⁵ D. J. Singh and C. H. Park, Phys. Rev. Lett. **100**, 087601 (2008).

¹⁶ A. Filippetti and N. A. Hill, Phys. Rev. B **65**, 195120 (2002).

¹⁷ S. Bhattacharjee, E. Bousquet, and P. Ghosez, Arxiv e-prints **811**, 0811.2344 (2008).

¹⁸ S. Bhattacharjee, E. Bousquet, and P. Ghosez, J. Phys.: Condens. Matter **20**, 255229 (5) (2008).

¹⁹ B. L. Chamberland, A. W. Sleight, and J. F. Weiher, J. Solid State Chem. **1**, 506 (1970).

- ²⁰ G. Kresse and J. Furthmüller, Phys. Rev. B **54**, 11169 (1996).
- ²¹ G. Kresse and D. Joubert, Phys. Rev. B **59**, 1758 (1999).
- ²² P. E. Blöchl, Phys. Rev. B **50**, 17953 (1994).
- ²³ P. E. Blöchl, O. Jepsen, and O. K. Andersen, Phys. Rev. B **49**, 16223 (1994).
- ²⁴ H. J. Monkhorst and J. D. Pack, Phys. Rev. B **13**, 5188 (1976).
- ²⁵ R. D. King-Smith and D. Vanderbilt, Phys. Rev. B **47**, 1651 (1993).
- ²⁶ D. Vanderbilt and R. D. King-Smith, Phys. Rev. B **48**, 4442 (1993).
- ²⁷ E. O. Wollan and W. C. Koehler, Phys. Rev. **100**, 545 (1955).
- ²⁸ S. Satpathy, Z. S. Popović, and F. R. Vukajlović, Phys. Rev. Lett. **76**, 960 (1996).
- ²⁹ W. E. Pickett and D. J. Singh, Phys. Rev. B **53**, 1146 (1996).
- ³⁰ R. Søndenå, P. Ravindran, S. Stølen, T. Grande, and M. Hanfland, Phys. Rev. B **74**, 144102 (pages 12) (2006).
- ³¹ K. Kunc and R. M. Martin, Phys. Rev. Lett. **48**, 406 (1982).
- ³² X. Gonze and C. Lee, Phys. Rev. B **55**, 10355 (1997).
- ³³ A. Togo, FROPHO, <http://fropo.sourceforge.net>.
- ³⁴ H. T. Stokes, D. M. Hatch, and B. J. Campbell, ISOTROPY (2007), <http://stokes.byu.edu/isotropy.html>.
- ³⁵ T. Kimura, T. Goto, H. Shintani, K. Ishizaka, T. Arima, and Y. Tokura, Nature **426**, 55 (2003).
- ³⁶ T. Goto, T. Kimura, G. Lawes, A. P. Ramirez, and Y. Tokura, Phys. Rev. Lett. **92**, 257201 (2004).
- ³⁷ A. Malashevich and D. Vanderbilt, Phys. Rev. Lett. **101**, 037210 (2008).
- ³⁸ K. R. Poeppelmeier, M. E. Leonowicz, and J. M. Longo, J. Solid State Chem. **44**, 89 (1982).
- ³⁹ Y. Syono, S. Akimoto, and K. Kohn, J. Phys. Soc. Jpn **26**, 993 (1969).
- ⁴⁰ A. Hardy, Acta Crystallogr. **15**, 179 (1962).
- ⁴¹ X. Marti, F. Sanchez, V. Skumryev, V. Laukhin, C. Ferrater, M. Garciaenca, M. Varela, and J. Fontcuberta, Thin Solid Films **516**, 4899 (2008).
- ⁴² P. A. Salvador, T.-D. Doan, B. Mercey, and B. Raveau, Chem. Mater. **10**, 2592 (1998).